

sponding diagram for the special transitions involving the  $j=0$  levels is immediately constructed from the Wolff selection rules given in Ref. 6.

<sup>2</sup>Because of the complexity of the Baraff Hamiltonian, the treatment in Ref. 12 is confined to  $k_H=0$ .

PHYSICAL REVIEW B

VOLUME 2, NUMBER 8

15 OCTOBER 1970

## Discrete Variational Method for the Energy-Band Problem with General Crystal Potentials\*

D. E. Ellis<sup>†</sup>

*Department of Physics, University of Florida, Gainesville, Florida 32601*

and

*Department of Physics, Northwestern University, Evanston, Illinois 60201*

and

G. S. Painter<sup>‡</sup>

*Quantum Theory Project, University of Florida, Gainesville, Florida 32601*

(Received 1 May 1970)

A general variational method for efficiently calculating energy bands and charge densities in solids is presented; the method can be viewed as a weighted local-energy procedure or alternately as a numerical integration scheme. This rapidly convergent procedure circumvents many of the difficulties associated with the evaluation of matrix elements of the Hamiltonian in an arbitrary basis and treats the general nonspherical potential with no more complication than the usual "muffin-tin" approximation. Thus the band structure of ionic and covalent materials can be calculated with realistic crystal potentials. As an example, the method is applied to the one-electron model Hamiltonian with a nonspherical local potential, using a linear combination of atomic orbitals basis. Matrix elements of the Hamiltonian are evaluated directly without decomposition into atomic basis integrals; no "tight-binding" approximations are made. Detailed calculations are presented for the band structure and charge density of bcc lithium which demonstrate the feasibility of our method, and reveal the sensitivity of the energy bands to nonspherical and exchange components of the crystal potential. Various prescriptions for the construction of crystal potentials are considered, and convenient least-squares expansions are described. The extension of these methods to nonlocal potentials such as are encountered in the Hartree-Fock self-consistent-field procedure is discussed.

### I. INTRODUCTION

The energy-band model for crystalline solids has proved to be very useful in describing optical, magnetic, and transport properties of a variety of materials. The success of this model depends essentially on the choice of potential in the one-electron effective Hamiltonian. This potential may be determined in many ways, including an empirical set of parameters, the superposition of model free-atom potentials, or by a self-consistent iterative procedure based on a many electron picture. Two inter-related problems which must be solved in applying the theory are (a) to find a crystal potential which adequately accounts for electron correlation and (b) to develop computational methods powerful enough to handle realistic potentials. The very great progress made in understanding the electronic structure of metals has been aided by the fact that the free-electron " $p^{1/3}$ " local exchange and the

"muffin-tin" spherical average potentials are rather good approximations to the crystal potential. Computational methods such as the augmented-plane-wave (APW), KKR, and Green's-function schemes<sup>1-3</sup> exploit this simple form of the potential. However, in some cases, particularly for nonmetals, the results have been found to be sensitive to nonspherical components of the potential and/or deviations from the simple exchange approximation.<sup>4,5</sup> In addition to studying these effects, it now appears important to investigate the consequences of adopting effective potentials, nonlocal as well as local, based on pseudopotential, Hartree-Fock, or more fundamental many-electron models.

The approximations which simplify the energy-band treatment of metals seem to be practically useless for most ionic and covalently bonded solids. The aspherical ion crystal fields and the covalent charge distributions are not well represented by a spherical average, and the exchange model is ques-

tionable because of extreme variations of density through the crystal cell. Methods which have been set up to exploit the ionic or atomic character of these materials, such as the orthogonalized-plane-wave (OPW) and linear-combination-of-atomic orbitals (LCAO) tight-binding schemes, have been rather successful in parametrizing the experimental data. However, development of these methods from the *ad initio* point of view has been rather slow, due primarily to the multicenter integral problem, familiar from molecular theory. Considerable effort has been spent in overcoming this computational problem.

A numerical-variational method for the energy-band problem with general crystal potentials is presented in Sec. II. The multidimensional numerical integration technique employed makes it possible to circumvent not only the integration difficulties inherent in ordinary energy-band calculations, but also the particular problems for nonspherical potentials. As an example, the method is applied to the LCAO tight-binding basis. Methods of constructing the crystal potential are discussed in Sec. III; convenient representations of the crystal potentials and charge density in various regions of the unit cell are presented and we show how these methods can be extended to include a nonlocal potential. In Sec. IV we present detailed calculations on the band structure and charge density of bcc lithium which demonstrate the feasibility of our method, and reveal the sensitivity of the energy bands to nonspherical and exchange components of the crystal potential.

## II. VARIATIONAL APPROACH

### A. One-Electron Model

Initially, we consider the application of these numerical methods to the variational solution of the Schrödinger equation with a one-electron Hamiltonian

$$H(\vec{r}) = -\frac{1}{2}\nabla^2 + V(\vec{r}) \quad (1)$$

where  $V(\vec{r})$  represents some approximation to the potential for an electron in the crystal. (All energies are given in Hartree atomic units  $e^2/a_0$  and lengths in Bohr radii  $a_0$ .)

In the linear variational approach, we seek approximate solutions expressible as

$$\Psi_i(\vec{k}, \vec{r}) = \sum_j \chi_j(\vec{k}, \vec{r}) C_{ji}(\vec{k}) \quad (2)$$

where the basis functions  $\chi_j$  are Bloch functions, i. e.,

$$\chi_j(\vec{k}, \vec{r}) = M^{-1/2} e^{i\vec{k}\cdot\vec{r}} U_j(\vec{k}, \vec{r}) \quad (3)$$

Here  $U_j$  is periodic in the lattice and the coefficients

$C_{ji}$  are parameters to be determined variationally.

In the Rayleigh-Ritz (RR) variational procedure, one obtains approximate wave functions  $\Psi_i$  and energies  $\epsilon_i$ , which are upper bounds to the exact eigenvalues of  $H\Psi_i = \epsilon_i\Psi_i$  by minimizing the expectation value of the operator  $(H - \epsilon)$  with respect to the coefficients  $C_{ji}$ . The upper-bound property is obtained by defining the expectation values  $\langle \Psi_i | H - \epsilon | \Psi_j \rangle$  as *integrals* over the spatial domain. The linear variational equations are found in the standard way by writing

$$\langle \Psi_i | H - \epsilon | \Psi_j \rangle = \sum_{m,n} C_{ni}^* \langle \chi_n | H - \epsilon | \chi_m \rangle C_{mj} \quad (4)$$

and requiring

$$\frac{\partial \langle \Psi_i | H - \epsilon | \Psi_j \rangle}{\partial C_{pq}} = 0 \quad (5)$$

leading to the secular matrix equation

$$H(\vec{k})C(\vec{k}) = \epsilon(\vec{k})S(\vec{k})C(\vec{k}) \quad (6)$$

where

$$H_{ij} = \langle \chi_i | H | \chi_j \rangle, \quad S_{ij} = \langle \chi_i | \chi_j \rangle.$$

The secular equation can be solved by standard methods; elements of the diagonal matrix  $\epsilon(\vec{k})$  form the familiar energy-band structure. The number of bands found simultaneously here coincides with the number of basis functions employed. The major difficulty in applying the RR method is the evaluation of matrix elements of the Hamiltonian, especially with a potential of general form. Some progress can be made by selecting simple basis functions  $\chi_j$ , e. g., plane waves; however, the resulting wave-function expansion (2) may prove slowly convergent.

Another approach is to modify the RR procedure; one variant of this method can be found by redefining the expectation value as a weighted sum of integrand values determined by some *discrete sampling* rule. While the upper-bound property is lost, one is freed from errors introduced by approximate evaluation of the integral matrix elements.<sup>6,7</sup> In a Bloch basis, it is easily shown that matrix elements of a lattice translation-invariant operator  $O(\vec{r})$  can be reduced to an integral over a single unit cell:

$$\langle \chi_i | O | \chi_j \rangle = \int_{\Omega} d^3r U_i^*(\vec{k}, \vec{r}) O(\vec{r}) U_j(\vec{k}, \vec{r}) \quad (7)$$

Accordingly, we redefine the expectation value as

$$\langle \chi_i | O | \chi_j \rangle = \sum_{m=1}^N \omega(\vec{r}_m) U_i^*(\vec{k}, \vec{r}_m) O(\vec{r}_m) U_j(\vec{k}, \vec{r}_m) \quad (8)$$

with weight function  $\omega(\vec{r})$  and sample points  $\{\vec{r}_m\}$  in the unit cell, and proceed again to derive a secular equation identical to Eq. (6). If the weighting function is chosen appropriately (see Appendix), the weighted sample will converge to the integral as the number of points is increased, and the procedure can be thought of as an internally consistent integration rule, as well as a weighted local-energy scheme. Either point of view can be adopted for the following discussion. Of course, there are a variety of variational procedures based on different error criteria, e.g., minimization of the operator  $|H - \epsilon|^2$  leads to a *least-squares* method of considerable interest.<sup>6,7</sup> At present, the additional computational effort required by this method seems unjustified.

### B. Bloch Basis Set

The variational approach outlined above is not restricted to a particular form of basis function; the choice of basis will be dictated by requirements of convergence (in basis size) and computational convenience. Accumulated experience shows that composite basis sets such as APW, OPW, and combined plane-wave tight-binding<sup>8</sup> forms are well suited for describing both atomic cores and the interatomic region of the crystal cell. However, recent work has shown<sup>9</sup> that even the simple LCAO tight-binding scheme is capable of high accuracy with a limited basis size when applied carefully. As an initial application,<sup>10</sup> we have chosen to implement the LCAO tight-binding basis

$$\chi_i(\vec{k}, \vec{r}) = M^{-1/2} \sum_{\nu} e^{i\vec{k} \cdot \vec{R}_{\nu}} a_i(\vec{r} - \vec{R}_{\nu} - \vec{\mu}_i) \quad (9)$$

with exponential Slater-type orbitals (STO)  $a_i$  of the form  $x^l y^m z^n r^p e^{-ar}$  located at each atomic site. Since a large number of atomic and molecular calculations have shown the utility of the STO basis, we are able to carry over readily available optimized atomic functions<sup>11</sup> as a starting point for the crystal calculation. In addition, this basis lends itself readily to further analysis, such as projection of localized (Wannier) functions and population analysis of ionicity, hybridization, and covalent bond densities.

There have been many previous applications of the tight-binding method; in the standard approach, one expands the matrix elements in (6), using (9), and attempts to evaluate the resulting multicenter molecular integrals. The difficulties of accurately evaluating the multicenter integrals are well known from molecular theory; moreover the lattice sum of component integrals which must be performed leads to further loss of accuracy. In early efforts, three-center and most two-center (next nearest neighbor, etc.) integrals were usually ignored, with subsequent poor results. This has tended to place the LCAO method in general disfavor as an *ab initio*

approach, and its main use has been as a semiempirical interpolation scheme.<sup>12</sup> If one adopts a simple analytic form for the potential, the multicenter integral problem can be solved, e.g., by the Gauss transform method,<sup>9,13</sup> and many former objections have been removed. Our numerical method has several additional advantages: (a) No specific analytic form is required for the potential; (b) no loss of accuracy is experienced due to lattice sums, since component molecular integrals are never generated; and (c) inexpensive preliminary studies are easily made with a small number of sampling points, to optimize the atomic basis and reveal gross features of the band structure.

## III. CRYSTAL POTENTIAL AND CHARGE DENSITY

### A. Crystal Potential

The many different types of potential<sup>1,4,5,14</sup> used for energy-band calculations have goals which cover a similar range, from correlating and fitting experimental parameters, to attempting to develop a base for a more fundamental many-electron theory of solids. Fortunately, we have progressed to the point where different methods yield equivalent results for the same model potential. Often, slight empirical adjustments to *a priori* potentials yield satisfactory fits to experimental data, e.g., Fermi surfaces and optical structure. A number of internally consistent APW and OPW calculations have now been made<sup>4,14</sup> by iterative refinements of the model potentials which suggest that the effective exchange potential must be reconsidered carefully. Similar evidence is found from non-self-consistent studies of transition-metal and rare-earth compounds<sup>15</sup>; however, the exchange effect here is mixed with the problem of the nonspherical crystal field. We shall not discuss the many proposed refinements and modifications of Slater's  $\rho^{1/3}$  effective-exchange potential,<sup>16</sup> which is in turn based on the Hartree-Fock model, except to note that each scheme requires detailed numerical investigation.

In order to verify that our method is accurate and efficient, we have chosen initially to implement the *ad hoc* local potential commonly used,

$$V(\vec{r}) = \sum_{\nu, i} V_i(\vec{r} - \vec{R}_{\nu} - \vec{\mu}_i) + V_x(\vec{r}) \quad , \quad (10)$$

consisting of superimposed atomic (or ionic) Coulomb potentials and the effective exchange  $V_x$ . The atomic Coulomb potentials are readily summed; ionic potentials are treated by separate summation procedures for point ion and overlapping ion contributions. Efficient summation procedures are available for point ion potentials.<sup>17,18</sup> The exchange potential is generated from the crystal charge density  $\rho^{1,1}(\vec{r})$  as

$$V_x^{\uparrow,\downarrow}(\vec{r}) = -3\alpha[(3/4\pi)\rho^{\uparrow,\downarrow}]^{1/3}, \quad (11)$$

where the arrows  $\uparrow, \downarrow$  denote either spin, and  $\alpha$  is a scaling parameter.<sup>19</sup> The assumed initial charge density is found by summing atomic densities,

$$\rho^{\uparrow,\downarrow} = \sum_{\nu,i} \rho_i^{\uparrow,\downarrow}(\vec{r} - \vec{R}_\nu - \vec{\mu}_i). \quad (12)$$

One iterative procedure to achieve self-consistency is to solve the band problem with the potential (10), occupy the Bloch states according to Fermi-Dirac statistics and determine densities of either spin, solve the Poisson equation for the Coulomb potential, redetermine the exchange potential via (11), recalculate the bands, etc.

It may be useful to comment on several approximations commonly made in applying the model potential (10).

(a) The muffin-tin approximation, which replaces (10) by its spherical average inside nonoverlapping atomic spheres of radius  $R_i$  and by a constant outside, is practically useless for ionic and covalent bonded materials, but seems quite good (to a few tenths of an eV) for simple metals. The error in a material like diamond amounts to several eV over a large region of the cell. The interatomic region can be treated relatively easily in both APW and OPW methods (warped muffin tin),<sup>5</sup> but the atomic sphere region is more difficult. In order to assess the effects of these approximations, we have developed fitting procedures and convenient analytic representations of the potential (10), which are discussed in Sec. IV.

(b) The model exchange potential (11) has often been approximated by the sum of atomic exchange potentials,

$$V_x'(\vec{r}) = -3\alpha \sum_{\nu,i} \frac{3}{4\pi} \rho_i(\vec{r} - \vec{R}_\nu - \vec{\mu}_i)^{1/3}, \quad (13)$$

which is the leading term in a multinomial expansion of (11). However, a significant error is made whenever the atomic charge densities overlap, and additional terms must be included. From the numerical point of view, this method of approximation has a further disadvantage in that lattice sums such as (13) are very slowly convergent, compared to (12).

For our direct method, the initial atomic (or ionic) Coulomb potential and charge density is obtained, for example, from a version of Herman and Skillman's HFS program<sup>20</sup> or from Clementi's analytic wave functions.<sup>11</sup> When the atomic potential and density are given in tabular form, a Lagrange interpolation procedure is used to provide a continuous representation. The crystal potential (10) is then summed to obtain  $V(\vec{r}_m)$  on the sample points

required in constructing matrix elements of the Hamiltonian.

In an alternative procedure, one uses the tabular values  $V(\vec{r}_m)$  over a grid in the unit cell to project out analytic (least-squares) representations of the potential which may then be used to form matrix elements. In this way, the effect of muffin-tin, warped muffin-tin, and other approximations can be studied. For this approach, we find it convenient to define a basis set orthonormal over a finite set of points

$$\varphi_j(\vec{r}) = \sum_{i=1}^L g_i(\vec{r}) W_{ij} \quad (14)$$

constructed as a linear combination of functions  $\{g_i\}$ . Let us define the inner product over a pair of functions  $a$  and  $b$  as

$$\langle a | b \rangle = \sum_{m=1}^N \omega(\vec{r}_m) a^*(\vec{r}_m) b(\vec{r}_m) \quad (15)$$

with weight function  $\omega(\vec{r})$  over the set of points  $\{\vec{r}_m\}$ ; then the orthonormality condition is simply  $\langle \varphi_i | \varphi_j \rangle = \delta_{ij}$ . The least-squares fit of a function  $V(\vec{r})$  is expressed simply as

$$V'(\vec{r}) = \sum_{j=1}^J \varphi_j(\vec{r}) \langle \varphi_j | V \rangle, \quad (16)$$

and freedom in the choice of  $\omega(\vec{r})$  allows the fit to be optimized in a given subspace of the fit region. While the fit (16) is unique, the basis functions  $\{\varphi_j\}$  are undetermined to within a unitary transformation. Preliminary fits made with Schmidt orthogonalized bases often proved troublesome because of approximate linear dependency among the functions  $\{g_i\}$ ; however, the canonical orthonormalization scheme<sup>21</sup> has proved quite satisfactory. In this scheme, the functions  $\varphi_j$  are labeled by eigenvalues of the diagonalized overlap matrix  $S$  ( $S_{im} = \langle g_i | g_m \rangle$ ) so that nearly degenerate functions corresponding to almost vanishing eigenvalues can be excluded from the basis set [thus,  $J \leq L$  in (14) and (16)]. The canonical functions are defined by

$$W_{ij} = U_{ij} \lambda_j^{-1/2}, \quad (17)$$

where  $U^* S U = \lambda$  is the diagonalized overlap matrix. Reasonably compact representations of the crystal potential can be found by dividing the unit cell into several regions: (a) nonoverlapping spherical volumes around each atom and (b) the volume outside all atomic spheres. A separate least-squares fit is generated inside each region; the fit is optimized by selecting basis functions appropriate for the behavior of the potential in each region. The accuracy of the fit within a given region also depends on the

weight function  $\omega(\vec{r})$ . One choice is to weight according to the volume element of integration, thus the fit optimization is shifted toward regions which make a large contribution to the matrix elements. Inside the atomic spheres, the fitting grid and weight factors are generated by the same scheme used in forming matrix elements of the Hamiltonian. Outside the spheres we use a uniform prismatic grid with uniform weighting.

To ensure that the potential fit has the correct symmetry, the functions  $\{\varphi_j\}$  are constructed from a symmetrized basis. Inside each atomic sphere we choose a localized set of functions  $\{g_i\}$  of the form  $r^p e^{-ar} A_{\Gamma\gamma}(\vec{Q})$ , where the  $A_{\Gamma\gamma}$  form basis functions for the totally symmetric irreducible representation of the point group at the atom site. In the intersphere region, we choose symmetrized plane waves generated from  $e^{i\vec{K}_\nu \cdot \vec{r}}$ , where  $\vec{K}_\nu$  are reciprocal-lattice vectors.<sup>3</sup> The muffin-tin approximation to the crystal potential is found simply by restricting the localized basis to spherically symmetric functions and by using only the  $K=0$  Fourier component outside the spheres. The warped muffin-tin model<sup>5</sup> is obtained by including nonzero wave vectors; thus this method of partitioning and choice of basis facilitates a study of the importance of various nonspherical contributions to the potential.

#### B. Representations of Charge Density

The crystal energy levels and wave functions are found numerically at a discrete set of wave vectors  $\{\vec{k}_i\}$ ; however, the calculation of physical properties such as x-ray (neutron magnetic) scattering factors require the charge density (spin density) of the form

$$\rho(\vec{r}) = \sum_{n, \vec{k}} f_n(\vec{k}) \Psi_n^*(\vec{k}, \vec{r}) \Psi_n(\vec{k}, \vec{r}) \quad (18)$$

(the  $f_n$  are occupation numbers) drawn essentially from the entire Brillouin zone. A useful procedure is suggested by rewriting (18), using (2) and (9) as

$$\rho(\vec{r}) = \sum_{\vec{k}} \sum_{jj'} G_{jj'}(\vec{k}, \vec{r}) Q_{jj'}(\vec{k}), \quad (19a)$$

where

$$G_{jj'} = \sum_{\nu} e^{i\vec{k} \cdot \vec{R}_\nu} a_{j'}^*(\vec{r}) a_j(\vec{r} - \vec{R}_\nu), \quad (19b)$$

$$Q_{jj'} = \sum_n f_n(\vec{k}) C_{j'n}^*(\vec{k}) C_{jn}(\vec{k}).$$

Here  $G$  is an invariant matrix depending only on the basis set;  $Q$  contains the results of the variational calculation, and may be called the "charge and bond order matrix."<sup>21</sup> Our operational procedure is to fit the matrix  $Q$  by an orthogonal set of functions

$$Q_{jj'} \approx \sum_i z_i(\vec{k}) \langle z_i | Q_{jj'} \rangle \quad (20)$$

and to complete the  $\vec{k}$  summation (integration) by a numerical sampling procedure.

#### C. Nonlocal (Hartree-Fock) Potentials and Exchange Density

The Hartree-Fock model has been used often in studying atomic and molecular structure; a few calculations on insulators<sup>21,22</sup> suggest that the model may have important applications in solids. Since the potentials must be determined self-consistently and are nonlocal, accurate Hartree-Fock energy-band calculations are an order of magnitude more difficult than those with an *a priori* potential. After each cycle of the iterative procedure, we must re-determine the charge density and Coulomb potential; in addition, we must calculate the exchange density (for either spin)

$$\rho(2|1) = \sum_{n, \vec{k}} f_n(\vec{k}) \Psi_n^*(\vec{k}, \vec{r}_2) \Psi_n(\vec{k}, \vec{r}_1) \quad (21)$$

required to generate the Hartree-Fock exchange potential

$$V_x(2|1) = \int d\tau_2 [\rho(2|1)/r_{12}] P_{12} \quad (22)$$

( $P_{12}$  is the permutation operator). Since the density is simply expressed as

$$\rho(2|1) = \sum_{\vec{k}} \sum_{jj'} G_{jj'}(\vec{k}, \vec{r}_2, \vec{r}_1) Q_{jj'}(\vec{k}) \quad (23a)$$

with

$$G_{jj'}(\vec{k}, \vec{r}_2, \vec{r}_1) = \sum_{\nu} e^{i\vec{k} \cdot \vec{R}_\nu} a_{j'}^*(\vec{r}_2) a_j(\vec{r}_1 - \vec{R}_\nu), \quad (23b)$$

we may conveniently evaluate the matrix elements of  $V_x$  by a numerical (six-dimensional) sampling procedure.

#### IV. CRYSTAL POTENTIAL, BAND STRUCTURE, AND CHARGE DENSITY OF bcc LITHIUM<sup>1</sup>

The success of the one-electron energy-band scheme for solids is largely dependent on the choice of model potential, and in the absence of complete experimental data one must rely on theoretical models. An atomic superposition model using the Slater exchange approximation has been favored by many workers.<sup>1</sup> However, computational approximations are usually made which make it difficult to assess the full possibilities of the model. The usual muffin-tin spherical averages to the potential and further simplifications of the exchange become questionable not only for ionic crystals, but also for some metals. One of the goals of this paper is to examine the superposition model carefully for the simplest and best understood metal, lithium, by comparison with the empirical Seitz potential which has been used successfully in many previous calculations.<sup>9,23,24</sup> Since recent work<sup>25</sup> has shown that the band structure depends somewhat on the parameterization of the exchange potential in the superposi-

tion model, and to a lesser degree, on nonspherical contributions, it may be useful to study these effects in more detail.

A second goal is to apply the discrete variational method (DVM) to the calculation of the energy bands, wave functions, and charge density of lithium metal for several assumed model potentials. Using LCAO basis sets, we show that the DVM is both accurate and rapidly convergent with respect to basis size and number of sample points. Since the DVM is a general numerical method, not restricted to muffin-tin or other approximations in the Hamiltonian, one can, for the first time, make use of the complete superposition model. Thus within a consistent computational scheme, we are able to compare the band structure determined by the empirical potential and the superposition model. After accounting for a uniform shift, one finds significant differences in the two sets of bands, as large as 0.02 Ry, occurring across the Brillouin zone. By recalculating the bands with a muffin-tin average of the superposition potential, we are able to show that the maximum contribution of nonspherical terms in the potential is 0.005 Ry.

One of the major advantages of our method is the ease with which wave functions and charge densities are obtained. These functions are required for any accurate prediction of experimentally interesting quantities such as optical absorption and x-ray scattering data; the analytic LCAO wave functions can be combined with efficient interpolation schemes to yield additional results. Furthermore, the charge (and exchange) densities can be used to generate self-consistent local (and nonlocal) potentials in an iterative calculation. In this paper, we give results for the charge density determined by the (non-self-consistent) superposition model; by comparing this density with the superposed atomic densities we extract the metallic bonding charge density. Preliminary results on self-consistent potentials are reported.

#### A. Crystal Potential

The Seitz empirical potential,<sup>26</sup> as quoted by Kohn and Rostoker,<sup>27</sup> has been the starting point for a number of recent calculations.<sup>9,23,24</sup> A least-squares fit to this muffin-tin potential of the form

$$V_s = \sum_{i=1}^9 C_i r^{i-2}, \quad r < R_s \quad (24)$$

$$V_s = V_0, \quad r > R_s$$

was given by Lafon and Lin<sup>9</sup>; the coefficients are reproduced for convenience in Table I. To obtain a direct comparison with earlier work, we have chosen the lattice constant  $a = 6.65$  a. u. for the bcc

phase of the metal (the experimental value at 78 °K is 6.597 a. u.<sup>28</sup>). The muffin-tin radius for tangent atomic spheres is thus  $R_s = 2.8795$  a. u.

The model potential formed by the superposition of free-atom Coulomb potentials and charge densities [cf. Eqs. (10) and (11)] taken by Rudge<sup>25</sup> as the starting point for self-consistent APW calculations, was constructed using the Herman-Skillman HFS<sup>20</sup> densities. The full Slater exchange ( $\alpha = 1$ ) was used, and a lattice sum over 58 neighboring atoms was found adequate to converge the potential in the unit cell to four significant figures. To make a comparison with the Seitz potential, a least-squares muffin-tin average [cf. Eq. (16)] of the form

$$V_{LO} = \sum_{i=1}^9 C_i r^{i-2} e^{-1.3r}, \quad r < R_s \quad (25)$$

$$V_{LO} = V_0, \quad r > R_s$$

was calculated, with coefficients given in Table I. This potential is plotted in Fig. 1(a), and is found to lie below the Seitz potential except for a small region near  $r = 1.5$ . Since  $V_{LO} < V_s$  over most of the crystal, we may expect to find a similar shift in the energy bands determined by either potential. The potential difference  $V_s - V_{LO}$ , shown in Fig. 1(b), can be minimized by scaling the exchange potential ( $\alpha < 1$ ). To study the effect of scaling, we have also calculated the model potential with  $\alpha = \frac{3}{4}$ ; the resulting potential difference is shown as a dashed line.

Nonspherical contributions to  $V_L$  reach a maximum near the muffin-tin radius and amount to about 1.5% of the total potential there. These terms will cause relative shifts of a few mRy in the band structure and thus, even in lithium, are important for modern "high-precision" calculations, quoting errors of 0.001 Ry or less. Although our band calculations on  $V_L$  use the numerical potential directly without the use of fitting procedures, it is useful

TABLE I. Least-squares coefficients for spherical average potentials.

	$V_s$	$V_{LO}$
$C_1$	-2.925 8671	-3.009 2561
2	+2.701 8157	-1.277 5884
3	+1.675 6787	+3.885 1735
4	-6.823 0630	-11.207 2550
5	+6.832 3735	+10.558 0710
6	-3.487 2725	-3.563 1211
7	+0.988 5456	-0.739 0967
8	-0.147 9572	+0.665 9503
9	+0.009 1263	-0.106 0555
$V_0$	-0.324 8	-0.395 42 a. u.

to have a simple picture of the nonspherical terms. The angular variation is well represented by  $L=4$  spherical harmonics, and in the  $z=0$  plane can be written as

$$\Delta V_L = A(r) \cos 4\varphi. \quad (26)$$

Values of the radial function  $A(r)$  are given in Table II; since the maximum in  $A(r)$  extends well inside the muffin-tin radius, we may conclude that the

TABLE II. Radial function  $A(r)$  for nonspherical contributions.

$r$	$A(r)$
0.5	$-1.0 \times 10^{-5}$
1.0	$-2.0 \times 10^{-4}$
1.5	$-1.2 \times 10^{-3}$
2.5	$-2.8 \times 10^{-3}$
2.88 (= $R_s$ )	$-2.8 \times 10^{-3}$
3.0	$-2.4 \times 10^{-3}$
3.325	$+4.0 \times 10^{-4}$

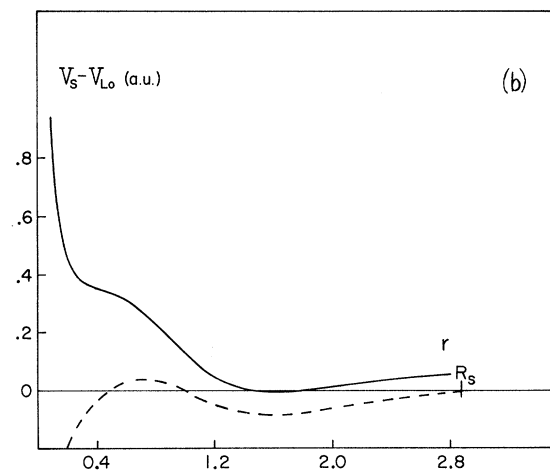
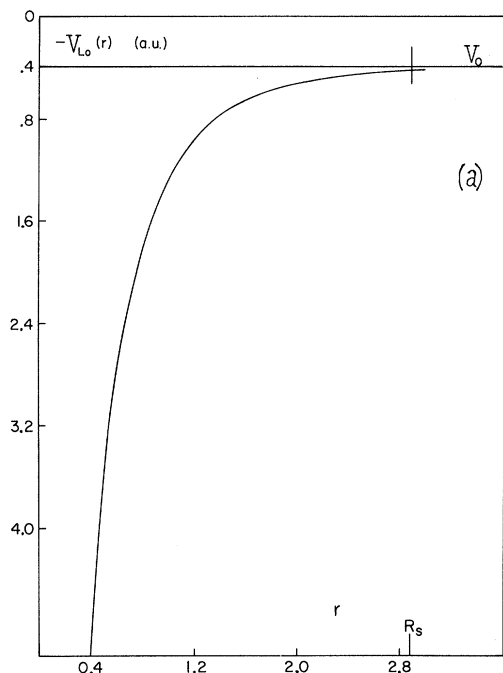


FIG. 1. (a) Spherical average potential  $V_{L0}$  formed by superimposing free-atom potentials and charge densities. The difference between  $V_{L0}$  and the Seitz potential  $V_S$  is shown in (b); full exchange is solid line,  $\alpha = \frac{3}{4}$  exchange is dashed line.

warped muffin-tin approximation<sup>5</sup> would be an inadequate representation of the potential.

#### B. Basis Sets and Convergence Properties

Convergence of the energy bands with respect to basis was studied by considering a number of LCAO Bloch basis sets [cf. Eqs. (2) and (9)]. Rather than attempting a systematic variation of atomic orbital exponents, we were guided by earlier tight-binding results<sup>9</sup> and Clementi's analytic wave functions<sup>11</sup> for the free atom. The atomic basis set  $B1$ , containing six functions listed in Table III, gives a rather accurate representation of the core level, conduction, and first excited bands over the entire Brillouin zone (BZ). The ten-function-extended bases  $B2$  and  $B3$  (Table III) yield slight improvements in the lower bands, but serve primarily to fill in additional excited  $sp$  bands. Basis sets  $B2$  and  $B3$  were also augmented by  $3s$ ,  $3p$ , and  $3d$  functions with results which show that the excited  $d$ -band structure can be treated adequately. An example of the convergence found at the point  $\Gamma$  in the BZ is given in Table IV, using the Seitz potential.

The energy levels were found to converge rapidly

TABLE III. Atomic basis functions.

$B1$

$$\begin{array}{l} 1s \\ 1s' \\ \left\{ \begin{array}{l} 2s \\ px \\ y \\ z \end{array} \right\} \end{array} \quad \begin{array}{l} e^{-2.43r} \\ e^{-4.51r} \\ \left\{ \begin{array}{l} r \\ x \\ y \\ z \end{array} \right\} \times e^{-0.66r} \end{array}$$

$B2 = B1$ , augmented by

$$\left\{ \begin{array}{l} 2s' \\ p'x \\ y \\ z \end{array} \right\} \quad \left\{ \begin{array}{l} r \\ x \\ y \\ z \end{array} \right\} \times e^{-2.43r}$$

$B3 = B1$ , augmented by

$$\left\{ \begin{array}{l} 2s' \\ p'x \\ y \\ z \end{array} \right\} \quad \left\{ \begin{array}{l} r \\ x \\ y \\ z \end{array} \right\} \times e^{-1.35r}$$

TABLE IV. Convergence in basis at  $\Gamma$ , 300 sample points.

State		Basis			Green's function (Ref. 2)
		B1	B2	B3	
(Ry)	$1\Gamma_1$	-3.764	-3.768	-3.766	
	$2\Gamma_1$	-0.676	-0.678	-0.682	-0.681
	$\Gamma_{15}$	+0.532	+0.530	+0.544	+0.506

TABLE V. Convergence with number of sample points.

State		Basis B1 Number of points			
		50	100	300	600
(Ry)	$1\Gamma_1$	-3.816	-3.768	-3.764	-3.764
	$2\Gamma_1$	-0.668	-0.672	-0.676	-0.674
	$\Gamma_{15}$	+0.526	+0.530	+0.532	+0.533

as the number of integration (sample) points was increased, and showed little dependence on the distribution and weights of these points. Both overlapping atomic distributions and muffin-tin sampling schemes (see Appendix) were tested with similar good results. Typical convergence data is shown in Table V, for the point  $\Gamma$ , using the basis  $B1$  with the Seitz potential. The uncertainty of about 0.002 Ry inferred for the 300 point sample is equal in magnitude to errors due to truncation of Bloch function lattice sums (carried out to a radius of 20 a.u.). The splitting of degenerate levels, such as  $\Gamma_{15}$ , due to accumulated error and the disymmetry of sample points, gives essentially the same error estimate.

### C. Energy Bands

#### 1. Seitz Potential

Rather extensive calculations of the energy bands for the Seitz potential were made, using the basis sets  $B1$ ,  $B2$ , and  $B3$ . The convergence found at general points in the BZ is essentially the same as found along symmetry lines, and for purposes of comparison we shall only discuss symmetry directions. The basis set  $B3$  represents a good compromise between simplicity and accuracy for the core, conduction, and first excited  $sp$  bands. (However,  $d$  states rapidly become important in the ex-

cited bands, particularly around the point  $H$  in the BZ.) The conduction bands and low-lying excited bands obtained with  $B3$  are drawn in Fig. 2; the conduction-band energies are compared (along the symmetry lines  $\Delta$ ,  $\Sigma$ , and  $\Lambda$ ) in Table VI with results obtained by different methods. Our energies obtained with 300 sample points, are in close agreement with the Green's-function calculation<sup>23</sup> and show an improvement over the results of Lafon and Lin,<sup>9</sup> obtained with a more restricted LCAO basis and the Gauss transform technique. The first excited band agrees well with that calculated by Williams,<sup>29</sup> using the KKR method.

#### 2. Superposition Model Potential

For purposes of comparison, energy bands determined by the three potentials  $V_S$ ,  $V_L$ , and  $V_{LO}$  were computed using the same basis ( $B1$ ) and integration scheme (300 points). These results show the sensitivity of the band structure to the assumed potential; as expected from the potential difference plot in Fig. 1(b), the Seitz bands lie at higher energy than those found for the model potential  $V_L$ . This shift is *not* uniform across the BZ; as one consequence, the energy gap at the zone face,  $E_g = E(N_1) - E(N'_1)$ , taken as an indication of aspherical distortions of the Fermi surface, is reduced from

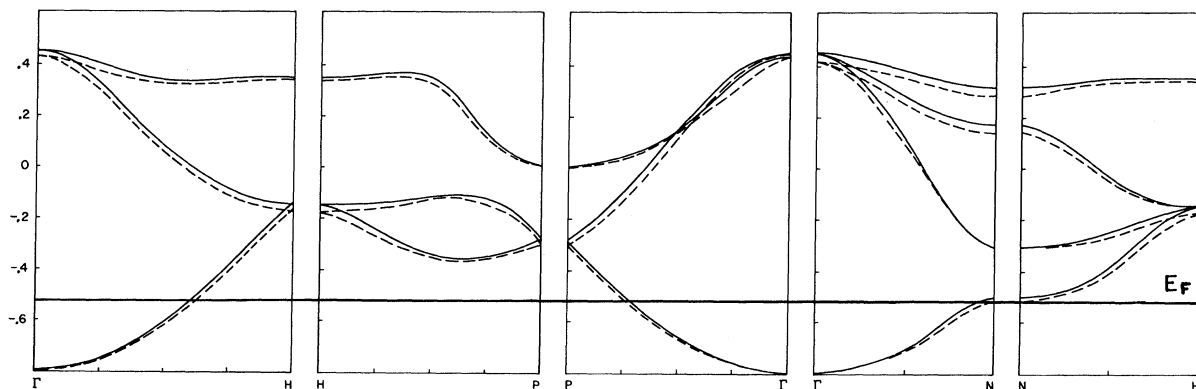


FIG. 2. Comparison of energy bands determined from the Seitz potential (solid line) and  $V_{LO}$  (dashed line), using the six function basis  $B1$ . The Seitz bands are shifted to bring the  $2\Gamma_1$  states into coincidence.



0.212 Ry for  $V_S$  to 0.198 Ry for  $V_L$ . The conduction and first excited  $sp$  bands for  $V_L$  are plotted along symmetry lines in Fig. 3. The Seitz bands (shifted by 0.114 Ry to bring the  $2\Gamma_1$  states into coincidence) are also drawn to show significant shifts across the entire BZ. These shifts become as large as 0.02 Ry, and clearly lead to a lowering of the Fermi energy relative to the Seitz value of  $E_F = -0.424$  Ry (or 0.258 Ry from the bottom of the conduction band) found by interpolation on a set of 30 inequivalent  $\vec{k}$  vectors. Since the Fermi level lies 0.01 Ry below the state  $N_1$ , there is no contact with the BZ boundaries.

Results obtained with the muffin-tin average potential  $V_{LO}$  agree closely with those found from  $V_L$  directly; the largest shift observed occurs at the point  $H$ , and is equal to 0.005 Ry. This limit on the effect of aspherical terms in the potential compares well with the results of Rudge<sup>25</sup>; however, to treat the cubic "crystal field effects" in the excited bands accurately, we must include  $d$  functions in the LCAO basis set.

#### D. Charge Density and Self-Consistent Potential

The crystal charge density  $\rho(\vec{r})$  was obtained as

$$\rho(\vec{r}) = \sum_i w_i \rho(\vec{k}_i, \vec{r}) \quad (27a)$$

with component densities [cf. Eq. (18)]

$$\rho(\vec{k}, \vec{r}) = \sum_n f_n(\vec{k}) |\psi_n(\vec{k}, \vec{r})|^2 \quad (27b)$$

calculated directly for 30 inequivalent  $\vec{k}$  vectors. The weights  $w_i$  are chosen proportional to the volume element of  $k$  space occupied, thus defining an integration rule. The simple shape of the Fermi surface and the very smooth variation of  $\rho(\vec{k}, \vec{r})$  with  $\vec{k}$  make more elaborate interpolation procedures unnecessary.

TABLE VI. Comparison of lithium conduction-band energies (lattice constant  $a = 6.65$  a.u.) calculated by different methods.

$ak/2\pi$	Energies (Ry)		
	Discrete variation (basis $B_3$ , 300 points)	LCAO Gaussian transform (Ref. 3)	Green's function (Ref. 2)
[100] $\Delta_1$			
0.0000	-0.682	-0.674	-0.681
0.2500	-0.640	-0.629	-0.640
0.5000	-0.512	-0.500	-0.512
0.6250	-0.414	-0.407	-0.414
0.7500	-0.290	-0.290	-0.294
1.0000	-0.062	-0.065	-0.061
[110] $\Sigma_1$			
0.2500	-0.598	-0.587	-0.598
0.3750	-0.498	-0.485	-0.497
0.5000	-0.414	-0.399	-0.412
[111] $A_1$			
0.1250	-0.650	-0.641	-0.651
0.2500	-0.556	-0.545	-0.556
0.3125	-0.486	-0.478	-0.486
0.3750	-0.400	-0.395	-0.400
0.5000	-0.192	-0.190	-0.191

The metallic bonding density was studied by comparing the calculated crystal density with the superimposed atomic charge densities; charge transfer along the  $(1, 1, 1)$  nearest-neighbor axis is shown in Fig. 4. The bonding charge is nearly constant over a considerable portion of the cell, as expected. The reduction of charge density near the metal nucleus, relevant for the contact part of the Knight shift, is evident; however, numerical values near the nucleus are not very accurate due to the limited basis size

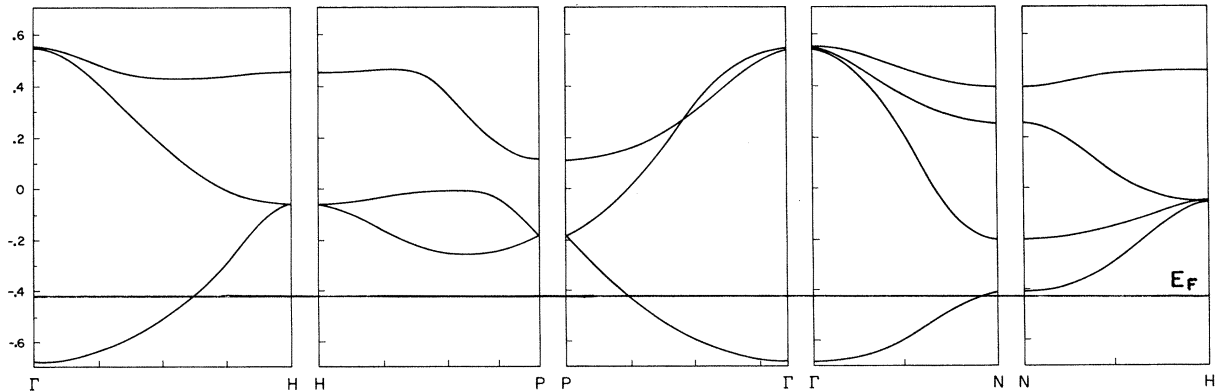


FIG. 3. Energy bands determined from the Seitz potential using the extended basis  $B_3$ . Tick marks on horizontal scale denote computed points.

and lack of self-consistency.

By an obvious extension of the superposition model, the self-consistent potential is defined as

$$V(\vec{r}) = V_C(\vec{r}) - 3\alpha[(3/8\pi)\rho(\vec{r})]^{1/3}, \quad (28)$$

where the Coulomb potential  $V_C$  is obtained from the crystal charge density  $\rho$  by solving the Poisson equation. In our approach to this problem, the density is fitted by a least-squares procedure to a composite basis set consisting of plane waves and localized (tight-binding) functions; the Poisson equation is then solved by a combination of numerical and analytic techniques. The results to date are encouraging (estimated errors in  $V_C$  of 1% with ~20 basis functions) and further work is in progress. Fits to the exchange density  $\rho(2|1)$  [cf. Eq. (21)] required for self-consistent Hartree-Fock calculations have also been generated to a few percent accuracy. We are evaluating several computational schemes for the matrix elements, to compare the relative merits of discrete sampling versus analytic integration procedures.

#### V. SUMMARY

We have combined numerical and variational techniques in formulating an energy-band procedure which is capable of treating general crystal potentials. The procedure has been specialized for treating nonspherical potentials in a tight-binding LCAO basis, and a number of calculations have been made to study the efficiency of this method. Detailed results were presented for the case of bcc lithium metal. The results of these calculations and those on diamond and graphite,<sup>30</sup> in two- and three-dimensional form, indicate that the method is flexible, efficient, and easily implemented. At the present level of development, the energy levels have been determined to 0.01 Ry or somewhat better with about 300 sample points per atom in the unit cell. These techniques are probably not competitive with the APW and KKR methods for determining a single energy band in metals, using a muffin-tin approximation. The discrete variational method proposed here has much to offer for systems in which nonspherical terms are important and/or a large number of bands are to be determined.

The results for lithium form part of a continuing study of effective potentials for the band model. Sensitivity of band structure to the assumed crystal potential was studied; differences between the empirical Seitz potential and the commonly prescribed *a priori* atomic superposition model were found to be more important than nonspherical contributions to the latter. Significant shifts in the bands as large as 0.02 Ry were found; in particular, the conduction-band width and Fermi energy was determined by the superposition model to be smaller than

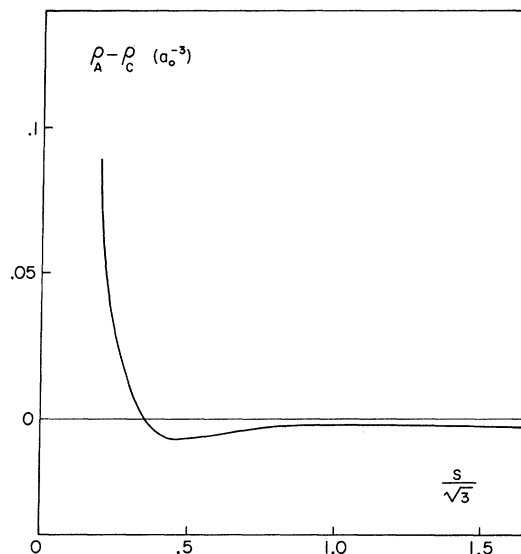


FIG. 4. Charge transfer  $\rho_A - \rho_C$  along the (1, 1, 1) nearest-neighbor axis from origin to bond center;  $\rho_A$  is the superimposed hfs free-atom density and  $\rho_C$  is the calculated crystal charge density.

that found for the Seitz potential. The metallic bonding charge and charge transfer from the atom were exhibited by comparing the calculated crystal charge density with superimposed atomic densities. Progress toward obtaining self-consistent Coulomb and exchange potentials was described.

An investigation of nonlocal potentials in the exchange problem becomes practically possible with this numerical approach. As a trial case, we are developing the Hartree-Fock potentials for iterative self-consistent calculations. While further work is required to develop an efficient computing scheme, preliminary results indicate that the exchange density can be obtained to sufficient accuracy.

#### ACKNOWLEDGMENTS

The authors wish to thank A. J. Freeman for helpful discussions, and R. W. Williams for providing us with results of his unpublished calculations. Computations were performed at the University of Florida Computation Center and at the Vogelback Computation Center of Northwestern University.

#### APPENDIX: NUMERICAL INTEGRATION PROCEDURE

The integration rule used here is essentially that described previously<sup>10,31</sup> in which the required matrix elements are reduced to integrals over the crystal unit cell, which are then evaluated by a systematic weighted sampling procedure. Thus for a periodic local operator  $O(r)$ ,

$$\begin{aligned}
 O_{ij}(\vec{k}) &= M^{-1} \langle \chi_i(\vec{k}, \vec{r}) | O(\vec{r}) | \chi_j(\vec{k}, \vec{r}) \rangle_M \\
 &= \langle \chi_i(\vec{k}, \vec{r}_0) | O(\vec{r}_0) | \chi_j(\vec{k}, \vec{r}_0) \rangle_0 \\
 &\simeq \sum_{m=1}^N \omega(\vec{r}_m) \chi_i^*(\vec{k}, \vec{r}_m) O(\vec{r}_m) \chi_j(\vec{k}, \vec{r}_m) ,
 \end{aligned}$$

where  $M$  denotes the repeating volume for periodic boundary conditions, the subscript 0 denotes a unit cell, and the points  $\{\vec{r}_m\}$  lie within this cell. The weighting function  $\omega(\vec{r})$  can be interpreted as the local volume per point, the inverse of the sampling point density function, and the integration rule as a weighted average of the local density  $\chi^* O \chi$ . This particular procedure when carried out consistently, yields high accuracy for surprisingly small effort.

The point density function which is used to generate the sample points  $\{\vec{r}_m\}$  represents a compromise between computational convenience and the desire to produce a stable rapidly convergent integration rule for the class of functions under discussion. Since we have to treat operators  $H$  with Coulomb singularities at each nucleus, and orbitals  $\chi_i$  with considerable nodal structure around each atomic site, it is apparent that a uniform point density will be far from optimum. We have found that a superposition of simple density functions based on each atom

$$\mu(\vec{r}) = \sum_g \mu_g(\vec{r}) = w^{-1}(\vec{r})$$

with the property

$$\mu_{\vec{r}-\vec{r}_g} \sim |\vec{r} - \vec{r}_g|^{-2}$$

gives good accuracy in the matrix elements. The results are relatively insensitive to the parameters governing  $\mu_g$ ; in fact, a muffin-tin model with uniform radial sampling inside each atomic sphere and uniform (prism) sampling in the interatomic region has some advantages. In the muffin-tin model, one can easily build in symmetry relations connecting different regions of the cell; on the other hand, with overlapping atomic distributions, one builds up the sample density along the atomic bonds, as well as about the individual atoms.

Finally, we may mention two useful symmetrization procedures: (a) As defined, the matrix  $O_{ij}$  will not be Hermitian in general; however, the symmetrized form  $O'_{ij} = O_{ij} + O_{ji}^*$  can be used to ensure that the eigenvalues of  $O$  are real. (b) It may be desirable to constrain the approximate Bloch eigenfunctions [Eq. (2)] to form basis functions for the irreducible representations of the crystal space group. This can be accomplished by choosing a symmetrized point set  $\{\vec{r}_m\}$  in the integration scheme, i. e., with each point  $\vec{r}$  include all points  $R\vec{r}$  with  $R$  symbolizing operations of the point group. Solution of the secular equation (6) will then produce the desired result, except for possibly degenerate states.

\*Research supported by the National Science Foundation, the Air Force Office of Scientific Research, and the Advanced Research Projects Agency through the Northwestern University Materials Research Center.

†Present address: Northwestern University, Evanston, Ill.

‡Present address: Metals and Ceramics Division, Oak Ridge National Laboratory, Oak Ridge, Tenn.

<sup>1</sup>*Methods in Computational Physics*, edited by B. Alder, S. Fernbach, and M. Rotenberg (Academic, New York, 1968), Vol. 8. This work reviews the current status of most energy-band methods.

<sup>2</sup>J. C. Slater, *Quantum Theory of Molecules and Solids* (McGraw-Hill, New York, 1965), Vol. II.

<sup>3</sup>J. Callaway, *Energy Band Theory* (Academic, New York, 1964).

<sup>4</sup>P. D. DeCicco, Phys. Rev. **153**, 931 (1967); L. F. Mattheiss, *ibid.* **181**, 987 (1969); W. E. Rudge, *ibid.* **181**, 1024 (1969).

<sup>5</sup>D. D. Koelling, A. J. Freeman, and F. M. Mueller, Phys. Rev. B **1**, 1318 (1970); D. D. Koelling, Phys. Rev. **188**, 1049 (1969).

<sup>6</sup>A. A. Frost, R. E. Kellogg, and E. C. Curtis, Rev. Mod. Phys. **32**, 313 (1960); D. H. Bell and L. M. Delves, J. Comput. Phys. **3**, 453 (1969); M. H. Lloyd and L. M. Delves, Int. J. Quantum Chem. **2**, 169 (1969); D. K. HARRISS and C. M. Carlson, J. Chem. Phys. **51**, 5458 (1969).

<sup>7</sup>Methods developed for explicitly correlated molecular wave functions include H. Conroy, J. Chem. Phys. **41**, 1331, (1964); **41**, 1336 (1964); **47**, 930 (1967); **47**, 5307 (1967); S. F. Boys, Proc. Roy. Soc. (London) **A309**, 195 (1969); S. F. Boys and N. C. Handy, *ibid.* **A309**, 209 (1969); **A310**, 63 (1969).

<sup>8</sup>A. B. Kunz, Phys. Rev. **180**, 934 (1969); F. A. Butler, F. K. Bloom, Jr., and E. Brown, *ibid.* **180**, 744 (1969).

<sup>9</sup>E. E. Lafon and C. C. Lin, Phys. Rev. **152**, 579 (1966).

<sup>10</sup>G. S. Painter and D. E. Ellis, Int. J. Quantum Chem. **3S**, 801 (1970).

<sup>11</sup>E. Clementi, IBM J. Res. Develop. Suppl. **9**, 2 (1965).

<sup>12</sup>J. C. Slater and G. F. Koster, Phys. Rev. **94**, 1498 (1954); G. Dresselhaus and M. S. Dresselhaus, *ibid.* **160**, 649 (1967).

<sup>13</sup>I. Shavitt, in *Methods in Computational Physics*, edited by B. Alder, S. Fernbach, and M. Rotenberg (Academic, New York, 1963), Vol. 2, p. 1.

<sup>14</sup>D. J. Stukel, R. N. Euwena, T. C. Collins, F. Herman, and R. L. Kortum, Phys. Rev. **179**, 740 (1969).

<sup>15</sup>T. M. Wilson, J. Appl. Phys. **40**, 1588 (1969); S. J. Cho, Phys. Rev. **157**, 632 (1967).

<sup>16</sup>J. C. Slater, Phys. Rev. **81**, 385 (1951); **165**, 658 (1968).

<sup>17</sup>M. P. Tosi, Solid State Phys. **16**, 1 (1964).

- <sup>18</sup>W. E. Rudge, Phys. Rev. 181, 1020 (1969).  
<sup>19</sup>J. C. Slater, T. M. Wilson, and J. H. Wood, Phys. Rev. 179, 28 (1969), and references therein.  
<sup>20</sup>F. Herman and S. Skillman, *Atomic Structure Calculations* (Prentice-Hall, Englewood Cliffs, N. J., 1963).  
<sup>21</sup>P. O. Löwdin, Advan. Phys. 5, 1 (1956).  
<sup>22</sup>L. P. Howland, Phys. Rev. 109, 1927 (1958); C. M. Sonnenschein, Ph. D. thesis MIT, 1965 (unpublished).  
<sup>23</sup>F. S. Ham, Phys. Rev. 128, 82 (1962), and references therein; 128, 2524 (1962), and references therein.  
<sup>24</sup>J. Callaway, Phys. Rev. 124, 1824 (1961).  
<sup>25</sup>W. E. Rudge, Phys. Rev. 181, 1024 (1969); 181, 1033 (1969).  
<sup>26</sup>F. Seitz, Phys. Rev. 47, 400 (1935).  
<sup>27</sup>W. Kohn and N. Rostoker, Phys. Rev. 94, 1411 (1954).  
<sup>28</sup>C. S. Barrett, Acta Cryst. 9, 671 (1956).  
<sup>29</sup>R. W. Williams (unpublished).  
<sup>30</sup>G. S. Painter and D. E. Ellis, Phys. Rev. B 1, 4747 (1970).  
<sup>31</sup>C. B. Haselgrove, Math. Comput. 15, 323 (1961); S. F. Boys and P. Rajagopal, Advan. Quantum Chem. 2, 1 (1965); H. Conroy, J. Chem. Phys. 47, 5307 (1967); D. E. Ellis, Int. J. Quantum Chem. 2, 35 (1968).

PHYSICAL REVIEW B

VOLUME 2, NUMBER 8

15 OCTOBER 1970

## Electrical Conductivity in Narrow Energy Bands\*

Robert A. Bari<sup>†</sup>

*Lincoln Laboratory, Massachusetts Institute of Technology, Lexington, Massachusetts 02173*

and

David Adler

*Department of Electrical Engineering,*

and

*Center for Materials Science and Engineering, Massachusetts Institute of Technology, Cambridge, Massachusetts 02139*

and

Robert V. Lange

*Physics Department, Brandeis University, Waltham, Massachusetts 02154*

(Received 24 February 1970)

The electrical conductivity for a system of electrons described by the single-band Hubbard Hamiltonian is studied. An expression for the electrical conductivity that is applicable in the narrow-band regime, i. e., the bandwidth  $\Delta$ , much smaller than intra-atomic Coulomb repulsion  $I$  is derived. It is shown that the conductivity vanishes at  $T=0$  to first order in  $\Delta/I$  for one electron per atomic site. For the non-half-filled-band case, the degeneracy of the (atomic limit) ground-state wave function plays a crucial role in yielding a nonzero value for the conductivity. The theory is used to analyze the experimental data in Li-doped NiO. It is demonstrated how, as a consequence of this theory, the contribution to the conductivity from the narrow  $3d^8$  band is suppressed in the total conductivity, contrary to an ordinary band-theory approach to the transport properties of this band.

### I. INTRODUCTION

Many transition-metal and rare-earth compounds are insulating despite the fact that elementary theory predicts that they have partially filled bands.<sup>1</sup> It was originally suggested by Mott<sup>2</sup> that materials with sufficiently narrow conduction bands are insulating, independent of the fractional occupancy of these bands. The failure of the Bloch-Wilson theory of conductivity in this case must be attributed to the neglect of electronic correlations. Mott<sup>2</sup> showed that for narrow bands, such as the  $d$  and  $f$  bands of transition-metal and rare-earth compounds, correlations can be expected to be particu-

larly strong. Hubbard and others have discussed a method for introducing the effects of electronic correlations into elementary band theory in a particularly simple manner, by considering correlations between electrons on the same ion cores only.<sup>3</sup> A model at least as sophisticated as this must be used if we want to understand quantitatively the electrical and optical properties of "Mott insulators."

In this paper we calculate the electrical conductivity of a system described by the Hubbard Hamiltonian<sup>3</sup> in the narrow-band regime. A formal definition of the electrical current is presented and the linear response to an external dc field is